19

Microwave Measurement

A. Dehé
Institut für Hochfrequenztechnik, Technische Universität Darmstadt

K. Beilenhoff
Institut für Hochfrequenztechnik, Technische Universität Darmstadt

K. Fricke
Institut für Hochfrequenztechnik, Technische Universität Darmstadt

H. Klingbeil
Institut für Hochfrequenztechnik, Technische Universität Darmstadt

V. Krozer
Institut für Hochfrequenztechnik, Technische Universität Darmstadt

H. L. Hartnagel
Institut für Hochfrequenztechnik, Technische Universität Darmstadt

Microwave measurements cover the frequency range from 0.5 GHz to about 20 GHz. Frequencies from 30 GHz to 300 GHz are often referred to as mm-waves. In the following, the most important measurements are described.

19.1 Power Measurement

Exact microwave power measurement is in demand for development, fabrication, and installation of modern telecommunication networks. It is essential for attenuation, insertion, and return loss measurements, as well as for noise measurement and six-port network analysis. This chapter gives a brief overview about the basics of microwave power measurement. Detailed information about this subject can be found in [1–4]. Power detectors usually consist of a sensor that transfers the microwave signal into a dc or low-frequency signal and a power meter to read out the measured power levels. The sensor includes a load impedance for the microwave source (Figure 19.1).

First, several power definitions need to be clarified:

- *Conjugate available power* (P_{CA}): The maximum available power a signal generator can transmit. This power is delivered by the generator if the load impedance is equal to the complex conjugate of the generator's source impedance. Since measurement techniques often require different lengths of waveguides or coaxial lines, the conjugate available power can be achieved only by tuning.
- Z_0 *Available power* (P_{Z0}): The power that is transferred via a coaxial line of characteristic impedance Z_0 into a load impedance Z_L equal to Z_0, while the generator has the impedance Z_G. Consequently, the available power level is reduced due to generator mismatch: $P_{Z0} = P_{CA}\,(1 - |\Gamma_G|^2)$, where Γ_G is

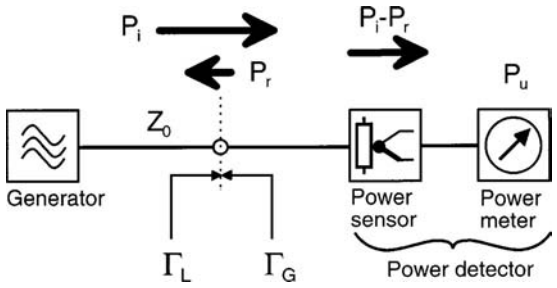

FIGURE 19.1 Setup of a power measurement in load configuration.

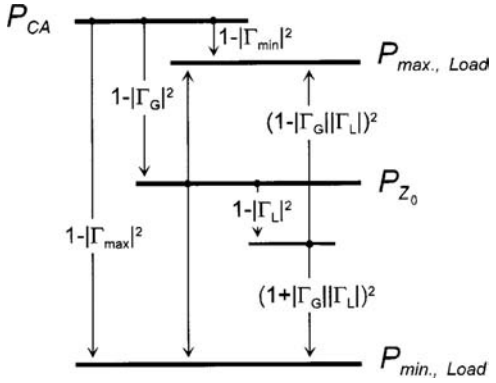

FIGURE 19.2 Relationships between conjugate power P_{CA}, Z_0 available power P_{Z0}, and the power levels available in the load of the power sensor.

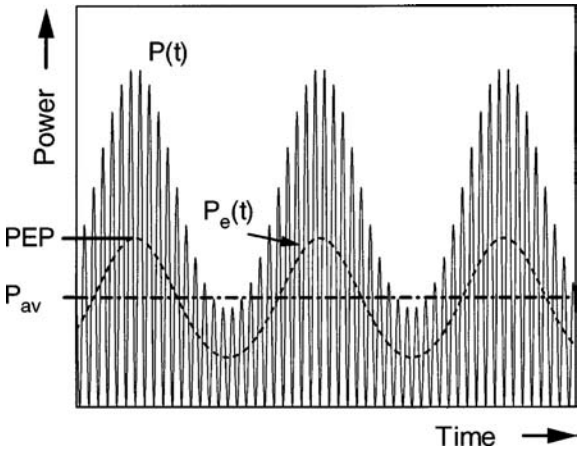

FIGURE 19.3 Power definitions for modulated signals.

the reflection coefficient of the generator. Figure 19.2 shows the relationships between P_{CA}, P_{Z0}, and the maximum and minimum power levels that can be measured in the load of a power sensor.

- *Average power* (P_{av}): The result of an averaging over many periods of the lowest modulation frequency of a modulated signal $P(t)$ (Figure 19.3).

- *Envelope power* ($P_e(t)$): The power averaged over the period of the carrier frequency.
- *Peak envelope power* (PEP): The maximum of $P_e(t)$.
- *Pulse power* (P_P): Defined for pulsed signals. If the pulse width τ and the repetition frequency $1/T$ is known, P_P is given by the measured average power:

$$P_p = P_{av}\frac{T}{\tau}$$

Measurement Errors and Uncertainties

Measurement errors occur due to mismatch as well as inside the power sensor and in the power meter. After correcting for these errors, the measurement uncertainties remain. Typically 75% of the total uncertainty belongs to mismatch and the smallest part is due to the power meter. The uncertainties and errors can be power dependent, frequency dependent, or independent of both. Of course, the *total uncertainty* must be calculated from the different uncertainties u_i as the root-sum-of-the-squares: rss = $\sqrt{\sum u_i^2}$, provided that the errors are all independent. A pessimistic error definition is the *worst-case uncertainty,* which simply sums up all extreme values of the independent errors.

Mismatch errors occur due to the fact that neither the generator (G), the line, nor the load (L) exhibit exactly the characteristic impedance Z_0. Using the modulus of the reflection coefficient $|\Gamma|$, the available power of the generator P_G can be expressed as [3]:

$$P_G = P_L\frac{\left|1-\Gamma_G\Gamma_L\right|^2}{\left(1-\left|\Gamma_G\right|^2\right)\left(1-\left|\Gamma_L\right|^2\right)} \tag{19.1}$$

The reflection coefficients can also be expressed in terms of the voltage standing wave ratio (VSWR):

$$|\Gamma| = \frac{\mathrm{VSWR}-1}{\mathrm{VSWR}+1} = \frac{Z_L - Z_0}{Z_L + Z_0} \tag{19.2}$$

As mentioned, the knowledge of Z_0 available power P_{Z0} is sufficient in most applications. Then the ratio between the Z_0 available power and the absorbed power is given by:

$$\frac{P_{Z_0}}{P_i - P_r} = \frac{\left|1-\Gamma_G\Gamma_L\right|^2}{1-\left|\Gamma_L\right|^2} \tag{19.3}$$

where the subscripts "i" and "r" denote the incident and reflected power, respectively. Expressing Equation 19.3 in dB gives the Z_0 *mismatch loss* while the term $-10\log(1-|\Gamma_L|^2)$ is called the *mismatch loss,* which accounts for reflected power from the load only.

Since the reflection coefficients are seldomly known completely but only their magnitudes are known, a *mismatch uncertainty* is defined as:

$$M_u = \left\{\left(1\pm\left|\Gamma_G\right|\left|\Gamma_L\right|^2\right)-1\right\}100\% \tag{19.4}$$

Conversion errors are due to the specific characteristics of the individual power sensor. The conversion efficiency is frequently dependent and a *calibration factor* (CF) is defined for each power detector:

$$\mathrm{CF} = \frac{P_u}{P_i} \tag{19.5}$$

where P_u is the uncorrected power and P_i is the actual incident power (Figure 19.1). Sometimes also the *effective efficiency* η_e is used:

$$\eta_e = \frac{P_u}{P_i - P_r} \tag{19.6}$$

Both quantities are related via the reflection coefficient of the load of the power sensor:

$$CF = \eta_e\left(1 - |\Gamma_L|^2\right) \tag{19.7}$$

The calibration factor is used to correct for efficiency loss and it also accounts for the mismatch loss. Still a remaining *calibration factor uncertainty* has to be taken into account. It is specified for each sensor. The calibration data are usually traceable to a national bureau of standards. Power sensors under test can be compared to the standards using high directivity couplers or power splitters [2].

The next described errors are due to the electronics inside the power meter.

Some power meters exhibit an internal reference oscillator to verify and adjust for the sensitivity of the diode or thermocouple sensor. The *reference power uncertainty* is specified by the manufacturer. Since this reference has its own reflection coefficient, it is related to a *reference oscillator mismatch uncertainty.*

Instrumentation uncertainty depends on the circuit limitations of the power meter and is specified by the manufacturer.

The *±1 Count Error* is for digital output and can be expressed by the relative power reading of the last significant digit.

Autozero can be used on all measurement ranges. Zero-setting immediately prior to the measurement can reduce *drift errors* when measuring in the lower ranges. Still, *zero set errors* remain due to noise during the zero-setting operation. This error can be very serious for measurement of low power levels [5]. *Zero carryover* is caused by ADC quantization errors in the zero readings for all measurement ranges except the most sensitive one. ADC quantization also causes a *power quantization error.* If very low power levels have to be measured, averaging can reduce random noise at the expense of measurement speed.

Power Sensors

A large variety of power sensors is available for the frequency range from dc up to 110 GHz and for minimum detectable power levels as low as 100 pW. The sensors differ in measurement principle and hence the correct choice depends on the application. A detailed description of power sensors is given in [2, 3]. Thermal sensors transform the absorbed microwave power into heat that is measured with temperature-sensitive elements:

- *Calorimeters* measure the heat absorbed in a fluid (e.g., water) of well-known specific heat. Applying the substitution principle, their precision can be enhanced. Because of their high stability, they are used in the National Institute of Standards. The manufacturer usually references the sensors to these standards.
- *Bolometers* and *thermistors* [3] make use of the temperature-dependent resistivity change of a resistive load, which is highly nonlinear. Hence, dc power substitution is used to keep the load at constant temperature. The substituted dc power is the measurement. Self-balancing bridges are used for this purpose but need careful ambient temperature compensation. The effective efficiency of bolometers is known very exactly. However, they have only relatively small dynamic range (typical 10 μW to 10 mW). Currently, liquid nitrogen-cooled, high-temperature superconducting bolometers with extremely high sensitivity of several thousands volts per watt are used [6]. A comprehensive overview of bolometers is given in [7].

- *Thermocouple sensors* are based on microwave power conversion into heat via a matched load impedance. Its temperature is controlled by thermocouples utilizing the thermoelectric effect in thin films or semiconductors [8]. One has to distinguish between realizations where the thermocouple itself represents the load impedance [3] and galvanically decoupled thermocouples [9]. The main advantages of the latter sensors are the better flatness of the response from dc to microwave and a lower VSWR. The design of such sensors is simple and a silicon micromachining technique can be applied to enhance the sensitivity [10]. The lowest measurable power levels are 1 μW.

Thermal sensors are well-suited to absolute power measurement, especially with respect to their high linearity. Their drawback is the relatively long response time (>10 ms), which limits these sensors to the measurement of average power. The high speed of Schottky diodes predestines them for the measurement of peak power, envelope power, and peak envelope power.

- *Diode sensors* consist of Schottky barrier diodes that are zero-biased and work in the square-law part of their *I–V* characteristics. For low power levels (<–20 dBm), these devices are very linear in response and measure the average power correctly. Still, diode sensors exhibit nonquadratic contributions [11], which can be important to account for when accurate measurement is required. Minimum detectable power is –70 dBm where the signal level is of the order of 50 nV and requires sophisticated amplification. The diode sensor is part of the sensors described below.
- *Peak power sensors* are specially designed for peak power measurements and account for measurement errors due to waveform and power level, although any diode detector can be used for this purpose if the peak voltages are ≤1 V.
- *Peak envelope analyzers* are designed to detect the envelope power. This is not possible with a simple diode sensor because the electronic setup of the diode must be different.
- *Feedthrough power sensors* are used to measure microwave power in transmission configuration. They have minor losses of approximately 0.5 dB and a limited bandwidth of typically 0.1 GHz to 1 GHz. The limiting device in these systems is a directional coupler with power splitters. Such a measurement can also be implemented with discrete elements. The characteristic figure of merit of these devices is the *directivity* (a_D), relating the read incident power P_i to the read reflected power P_r in case of reflection free load ($\Gamma_L = 0$):

$$a_D = 10 \log \frac{P_i}{P_r} [\text{dB}] \tag{19.8}$$

The directivity should be as high as possible.

The above power sensors are discrete devices. The maturity in microwave monolithic integrated circuit (MMIC) design and fabrication allows the integrated realization of diode power sensors; for example, in an integrated six-port reflectometer [12]. Activities to fabricate thermal power sensors integrable to MMIC-typical processes [13] can presently be implemented on commercial processes, such as the Philips Lemeill HEMT processes with additional postmicromachining [14].

Commercially Available Power Measurement Systems

A collection of different power sensors and corresponding measurement units is shown in Table 19.1. All power meters have GPIB interfaces for easy use in automated measurement.

19.2 Frequency Measurement

Frequency measurement in the microwave regime is usually part of a more complex measurement procedure, for example, determining the scattering parameters and filter characteristics of a DUT. If one

TABLE 19.1 Available Commercial Power Sensors and Power Meters

Supplier	Power sensor *Power meter	Frequency range	Dynamic range	VSWR	Remark	~Price $U.S.
			Power Sensors in Matched Load Configuration and Related Power Meter			
Hewlett-Packard	HP8478B	10 MHz–18 GHz		1.1–1.75	Thermistor	
Rohde & Schwarz	NRV-Z52	Dc–26.5 GHz	1 μW–100 mW	1.11–1.22	Thermocouple, up to 30 W available	1790
Marconi	6913/6914S	10 MHz–26.5/46 GHz	1 μW–100 mW	1.1–1.4/3.6	Thermocouple, up to 3 W available	3000/3900
Boonton	51100(9E)	10 MHz–18 GHz	10 μW–100 μW	1.18–1.28	Thermocouple	
Hewlett-Packard	HP8485A	50 MHz–26.5 GHz	1 μW–100 mW	1.10–1.25	Thermocouple	
	HP8487A	50 MHz–50 GHz	1 μW–100 mW	1.10–1.50	Thermocouple	
	HPR/*Q*/W8486A	26.5–40/33–50/75–110 GHz	1 μW–100 mW	1.4/1.5/1.08	Rectangular waveguide, thermocouple	
Rohde & Schwarz	NRV-Z6	50 MHz–26.5 GHz	1 nW–20 mW	1.2–1.4	Diode	1980
Marconi	6923/6924S	10 MHz–26.5/46 GHz	0.1 nW/0.1 μW–10 μW	1.12–1.5/3.6	Diode	4300/5000
Hewlett-Packard	HP8487D	50 MHz–50 GHz	0.1 nW–10 μW	1.15–1.89	Diode	
Rohde & Schwarz	*NRVS/D	Dc–26.5 GHz	0.4 nW–30 W		One/two channel	2710/5290
Boonton	*4230A	10 kHz–100 GHz	0.1 nW–25 W			
Marconi	*6960B	30 kHz–46 GHz	0.1 nW–30 W			6900
	*6970	30 kHz–46 GHz	0.1 nW–30 W		Hand portable	3800
Hewlett-Packard	*HP437B	100 kHz–110 GHz	0.07 nW–25 W			
			Power Analyzer			
Hewlett-Packard	HP84812/13/14A	500 MHz–18/26.5/40 GHz	0.6 μW–100 mW	1.25–1.60	Resolution 100 ps	
	*HP8991A	500 MHz–40 GHz	0.5 μW–100 mW		Rise/fall time 5 ns	
			Peak Power Sensors and Related Power Meter			
Rohde & Schwarz	NRV-Z31/33	0.03–6 GHz	1 μW–20 mW/1 mW–20 W	1.05–1.33	With NRVS	2020/2500
Hewlett-Packard	HP84812/3/4A	500 MHz–18/26.5/40 GHz	1 μW–100 mW	1.25/1.35/1.50		
Boonton	56340	500 MHz–40 GHz		1.25–2.00	Dual diode risetime <15 ns	
	*HP8990A	500 MHz–40 GHz				
Boonton	4500A	1 MHz–40 GHz	0.1 μW–100 mW			
			Feedthrough Power Sensor and Related Power Meter			
Rohde & Schwarz	NAS-Z7	1.71–1.99 GHz	0.01–30 W	<1.15	a_D > 26 dB, GSM, DCS1800/1900	1250
	*NAS	0.001–1.99 GHz	10 mW–1200 W			1120

TABLE 19.2 Digital Microwave Frequency Counter

Supplier	Counter	Frequency range	Resolution	Sensitivity	Remark	~Price $US
Hewlett-Packard	HP5351B	26.5 GHz	1 Hz	–40 dBm		7,500
Hewlett-Packard	HP5352B	40(46) GHz	1 Hz	–30 dBm		11,800

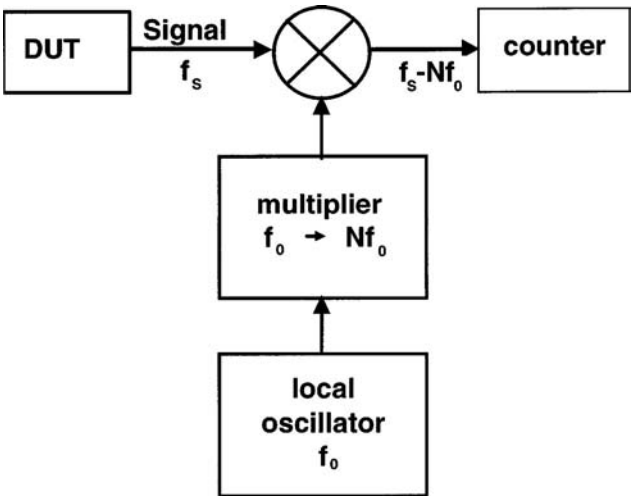

FIGURE 19.4 Block diagram of a digital frequency counter.

is only interested in frequency or a higher accuracy is required, one must use direct frequency measurement systems.

Two different techniques can be distinguished. The rather old-fashioned way is to use mechanically tunable resonators, the so-called *wave meters*. These are not explained in detail here. *Digital frequency counters* are an alternative and are now the state of the art (Table 19.2).

The digital frequency counter measurement system is based on the principle of counting the zero crossovers of a continuous sinusoidal signal. At low frequencies, this method can be used directly; whereas in the microwave region, direct digital counters are not available because of their limited bandwidth. Thus, a modified measurement system must be used.

The standard digital frequency counter usually consists of a mixer, a local oscillator (frequency f_0) in the lower frequency regime, several multipliers, and the digital counter. The principal measurement technique is shown in Figure 19.4.

An extremely stable local oscillator (quartz oscillator) is used to provide the reference signal used in the measurement system. This signal is multiplied by a factor of N and mixed with the RF signal of the DUT. The IF in the low-frequency range can be easily counted and, thus, the frequency of the signal f_s can be calculated according to the following equation.

$$f_s = f_{IF} + Nf_0 \tag{19.9}$$

For this method, an extremely stable low-frequency oscillator (often temperature controlled) must be provided and, in order to allow a sufficient bandwidth, a high number of multipliers must be implemented in this system.

A pulsed oscillator with extremely short risetime can circumvent this problem. In the frequency domain, this signal is given by spectral lines at $f = if_0$, where f_0 denotes the fundamental frequency of the pulses. Using a bandpass filter, a single frequency can be separated and transferred to the mixer.

19.3 Spectrum Analysis

The expression spectrum analysis subsumes the measurements that are performed to obtain the Fourier transformation $S(f)$ of a given signal $s(t)$. The Fourier transformation of $s(t)$ in the frequency domain is defined by the equation:

$$S(f) = \int_{-\infty}^{+\infty} s(t) e^{-j2\pi ft} \mathrm{d}t \tag{19.10}$$

In practice, the lower and upper bounds of the integral are limited by a finite measurement time that must be fixed by the user.

For the analysis of an unknown spectrum, different methods can be distinguished:

- *Wave analyzers and selective voltmeters:* These devices utilize a tunable filter for frequency-selective measurements.
- *Spectrum analyzers* rely on the principle of heterodyne mixing with subsequent bandpass filtering.
- Calculation of the spectrum using a *fast Fourier transformation* (FET). This method can be employed only for lower frequencies, since a digital-to-analog converter is needed. For microwave frequencies, the calculation of the spectrum using the FFT is, therefore, difficult to realize.

Since the spectrum analyzer is most suitable for microwave frequencies, it will be described in detail in the following. Brief introductions into the spectrum analyzer measurement techniques are given in [15, 16].

Spectrum Analyzer

The spectrum analyzer is most suitable for the analysis of microwave signals. It is a general-purpose instrument for measurements in the frequency domain and provides the user with the amplitude, power, or noise density of a signal depicted vs. the frequency. The frequency scale is in most cases linear; the vertical axes can be either linear or logarithmic. Spectrum analyzers are available from a few hertz up to more than 100 GHz. They give a quick overview of the spectral power distribution of a signal. Spectrum analyzers have a large dynamic range, a resolution bandwidth of a few hertz, and a reasonable frequency resolution.

The spectrum analyzer is suitable for the following measurements:

- *Measurement of absolute and relative frequency:* Frequency drift (unstabilized oscillators), spectral purity, and frequency of harmonics.
- *Absolute and relative amplitude:* Gain of frequency multipliers, harmonics of periodic signals, intermodulation (IM) distortion, and harmonic distortion.
- *Scalar network analysis* (*if equipped with a tracking generator*)*:* Frequency response of amplifiers and filters.
- *Electromagnetic interference* (*EMI*) *measurements:* Broadband spectra.
- *Measurements of modulated signals:* AM, FM, or PM.
- *Noise:* Many spectrum analyzers can be used for noise measurements of active devices.
- *Phase noise:* Phase noise of oscillators can be analyzed with spectrum analyzers [17].

Spectrum Analyzer Setup

The spectrum analyzer is basically an electronically tunable filter that allows the measurement of the amplitude, power, or noise at a certain frequency. Using the example shown in Figure 19.5, the principle of operation can be explained as follows.

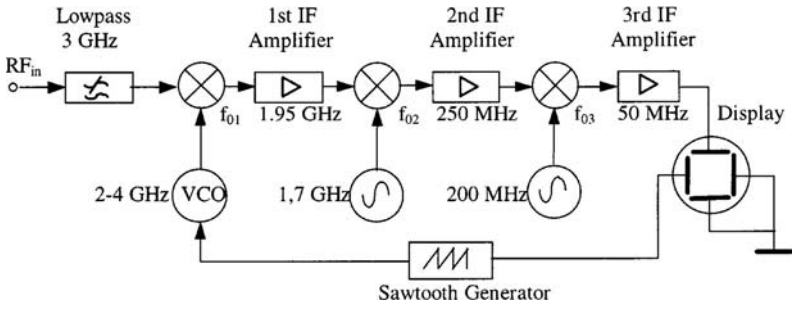

FIGURE 19.5 Simplified setup of a spectrum analyzer.

The tunable filter used to separate the frequencies to be measured is realized using a chain of mixers and IF amplifiers. In this case, three mixers convert a given input signal frequency f_s to the IF passband of the last IF amplifier. At least one of the oscillators is tunable (VCO) in order to scan the input frequency f_s. Sometimes, more than one tunable oscillator is used.

The first mixer and the following IF amplifier with a bandpass center frequency of 1.95 GHz in the given example selects the input frequency to be analyzed according to:

$$f_s = f_{o1} - 1.95\ \text{GHz} \tag{19.11}$$

The input frequency for the spectrum analyzer shown in Figure 19.4 can be due to the scan of the frequency of the tunable oscillator f_{o1}, between 50 MHz and 2.05 GHz. However, the image frequency f_{is} will also be mixed to the IF:

$$f_{is} = f_{o1} + 1.95\ \text{GHz} \tag{19.12}$$

Since f_{is} is in the range of 3.95 GHz to 5.95 GHz, a bandpass filter with a cut-off frequency of 3 GHz is used at the input to reject the image frequency.

Because it is difficult to realize a narrow bandpass at 1.95 GHz, the signal is converted to a lower frequency in the megahertz range. At these frequencies, stable quartz filters with high-quality factors can be employed. In principle, the RF frequency could be mixed down to the last IF section in one step. However, in such an arrangement, it would be difficult to suppress the image frequencies. In any case, the image frequency of each stage should be rejected by the preceding IF amplifier as shown in Figure 19.6 for the second stage of the given example.

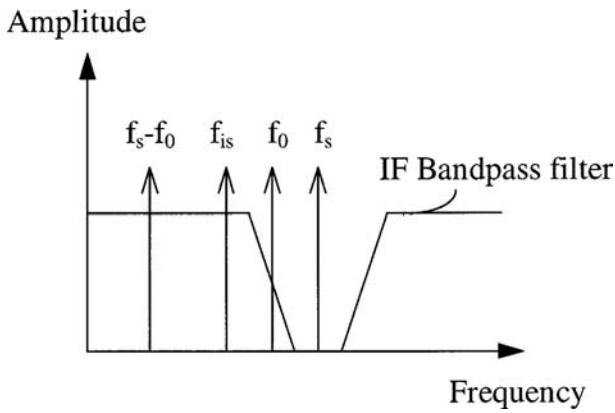

FIGURE 19.6 Example for the blocking of the image frequency by the IF filter in an arrangement according to Figure 19.5.

The last IF amplifier is very important for the performance of the complete system. In nearly all spectrum analyzers, its bandwidth — the so-called resolution bandwidth — can be adjusted in steps. For separation of closely spaced spectral components, the bandwidth should be very small. Most spectrum analyzers offer a minimum bandwidth of a few hertz. On the other hand, larger bandwidths are needed, since for a narrow IF filter only a slow scan speed can be allowed (see below) and, therefore, the measurement over several frequency decades would result in a large sweep time. The shape of the IF filter is important for the capability of the spectrum analyzer to separate close spectral components. The performance of the IF filter is described by the shape factor. It is defined by the ratio of the 60 dB to the 3 dB bandwidth of the IF filter. The IF filter can be switched between linear and logarithmic amplification. This is performed numerically in most cases.

A sawtooth generator produces the control voltage for the voltage-controlled oscillator (VCO) and the *x*-deflection voltage of the screen. A significant error is introduced in the frequency scale by a not-ideal voltage-to-frequency characteristic of the VCO. Therefore, in many cases, synthesizers with a quartzstabilized phase-locked loop [18] are used.

The detector has to be sensitive either to the amplitude, the power, or the noise ($\mathrm{mV}\sqrt{\mathrm{Hz}^{-1}}$). In a modern spectrum analyzer, digital signal processing is used for this purpose.

It is important to note that there are restrictions on the minimum sweep time T_s. In order to avoid settling errors of the narrow band pass IF amplifier with bandwidth B, the scan time should be for a frequency span S larger than [19, 20]:

$$T_s > 20S/B^2 \tag{19.13}$$

Most of the spectrum analyzers control the scan time automatically according to this equation.

Harmonic Mixing

For higher frequencies, the harmonic mixing technique is widely used. If the first 3-GHz low-pass filter in Figure 19.5 is omitted and the VCO produces harmonics, a larger number of input frequencies are converted to the passband of the spectrum analyzer. For the example shown, the possible input signals are depicted in Figure 19.7 vs. the VCO frequency according to:

$$f_s = nf_{01} \pm 1.95\ \mathrm{GHz} \tag{19.14}$$

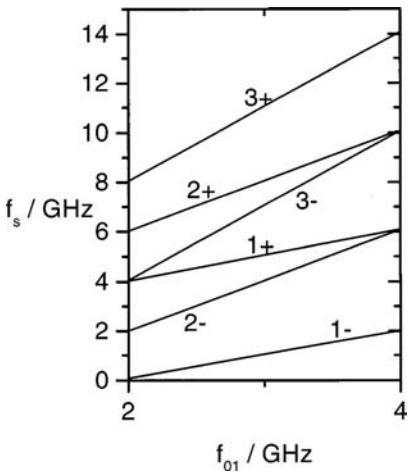

FIGURE 19.7 Measured RF frequency f_s vs. the frequency of the VCO (voltage-controlled oscillator) f_{01}. Parameters are n and the plus or the minus sign in Equation 19.4.

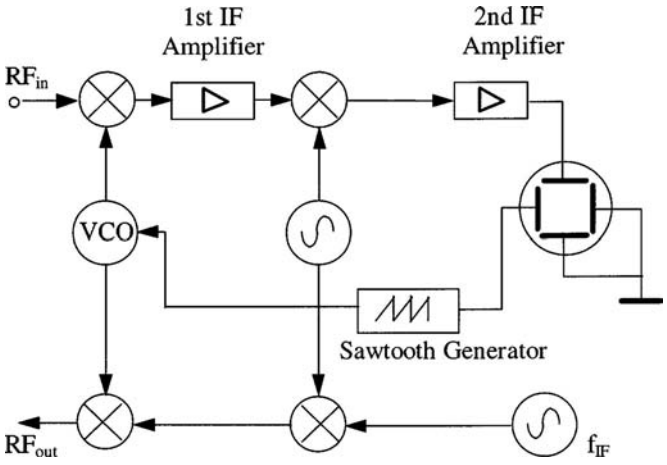

FIGURE 19.8 Principle of a tracking generator, which delivers at the port RF_{out} a signal that is precisely in the passband of the spectrum analyzer.

The notation of the numbers in the figure are the harmonic number n and the plus or the minus sign in the above equation. For a frequency f_{o1} = 3 GHz of the VCO, the following frequencies will appear at the same frequency location on the screen: 1.05 GHz (1–), 4.95 GHz (1+), 4.05 GHz (2–), 7.95 GHz (2+), 7.05 GHz (3–), 10.95 GHz (3+). A tracking preselection filter (see below), which is scanned with the VCO, can select one of these harmonics.

For further extension of the frequency in the upper mm-wave range, external mixers are used. With such an arrangement, frequencies higher than 500 GHz can be measured. Additionally, equipment for mixing of signals in the optical range is offered by some companies.

Tracking Preselection

For small input signals, the spectrum analyzer can be considered a linear device. However, if the input level increases, harmonics and intermodulation products are generated due to the nonlinearities of a mixer. These products result in spurious signals on the screen of the spectrum analyzer. In addition, image frequencies will appear on the screen, as demonstrated above. To avoid these spurious responses, a tracking preselection filter is employed at the input of the spectrum analyzer. A tracking preselection filter is an electronically tuned bandpass filter usually realized using a YIG filter.

Tracking Generator

Spectrum analyzers are often equipped with a tracking generator. The principle is shown in Figure 19.8. A local oscillator, with a frequency exactly on the center frequency of the IF amplifier, is mixed by an identical setup as in the analyzer path. Using the same local oscillator as in the analyzer path ensures that the frequency of the tracking generator follows precisely the center frequency of the swept window of the analyzed frequency band.

The tracking generator can be used for network analysis. If the tracking frequency is used as an input signal of a two-port, the amplitude of the output can be measured with the spectrum analyzer. Such a network analyzer has the advantage of being sensitive only in a very narrow band. Thus, third-order intermodulation products and noise are suppressed. However, only scalar measurements can be performed.

Commercially Available Spectrum Analyzers

A number of commercially available, general-purpose spectrum analyzers for the microwave and mm-wave range are listed in Table 19.3. Only a small number of spectrum analyzers available on the market

TABLE 19.3 Commercially Available Spectrum Analyzers

Company/ model	Frequency range	Min. res. bandw.	Amplitude accuracy	Remarks	Price $U.S.
Anritsu					
MS2602A	100 Hz–8.5 GHz		1.1 dB		30,600
Avantek					
3365	100 Hz–8 GHz	10 Hz		Portable, tracking	58,000
3371	100 Hz–26.5 GHz	10 Hz		Portable, tracking	66,000
R3272	9 kHz–26.5 GHz	300 Hz	1 dB	External mixer 325 GHz	38,000
Hewlett-Packard					
HP4196A	2 Hz–1.8 GHz	1 Hz	1 dB		
HP8590L	9 kHz–1.8 GHz	1 kHz	1.7 dB		9,080
HP8560E	30 Hz–2.9 GHz	1 Hz	1.85 dB	Portable	27,530
HP8596E	9 kHz–12.8 GHz	30 Hz	2.7 dB		25,090
HP8593E	9 kHz–22 GHz	30 Hz	2.7 dB		27,435
HP8564E	9 kHz–40 GHz	1 Hz	3 dB		50,890
HP8565E	9 kHz–50 GHz	1 Hz	3 dB		67,245
Marconi					
2370	30 Hz–1.25 GHz	5 Hz	5 Hz	With frequency extender	
2383	30 Hz–4.2 GHz	3 Hz	1 dB	Tracking	
Rohde & Schwarz					
FSEA30	20 Hz–3.5 GHz	1 Hz	1 dB		43,000
FSEB30	20 Hz–7 GHz	1 Hz	1 dB		52,000
FSEM30	20 Hz–26.5 GHz	1 Hz	1 dB	External mixer 110 GHz	64,000
Tektronix					
2714	9 kHz–1.8 GHz	300 Hz	2 dB	AM/FM demodulation 50 Ω/75 Ω	
2784	100 Hz–40 GHz	3 Hz	1.5 dB	Counter 1.2 THz, external mixer 325 GHz	

are presented. Most of the companies offer special equipment for production quality control. These spectrum analyzers can be computer controlled for fixed measurement routines. On request, spectrum analyzers with special options like fixed frequency operation, multichannel operation, support of external mixers, integrated frequency counters, and digital storage are available.

Typical specifications of microwave spectrum analyzers include:

- The frequency span is several gigahertz.
- With external mixers, the upper frequency limit can be extended to more than 100 GHz.
- The frequency accuracy is between 10^{-5} and 10^{-7}.
- The resolution bandwidth (i.e., the effective bandwidth of the narrow IF filter) can be adjusted in steps between 1 Hz and a few megahertz.
- The resolution bandwidth shape factor is typically 10:1.
- The amplitude accuracy is about 1 dB.
- The noise floor is at about –140 dBm.

19.4 Cavity Modes and Cavity *Q*

Cavities are used in a variety of applications. For example, they can be used to construct filters and they serve as those elements in microwave generators (e.g., klystrons) that determine the operating frequency. Cavities can also be applied in order to measure the frequency or the wavelength of microwaves (wavemeter). The most important parameters of a cavity are its resonant frequency and its q-factor. The latter determines the sharpness of the resonance, or, in case of filters, the bandwidth of the passband.

A cavity can be defined as a volume that is almost completely surrounded by a metallic surface. At one or two positions, coupling elements are applied to the metal surface in order to connect the cavity to other circuit elements. In the case of one coupling element, one speaks of a single-ended cavity; whereas

a transmission cavity has two coupling elements. The coupling elements are usually small compared to the dimensions of the cavity. The inside of the cavity is filled with dielectric material (e.g., air: $\varepsilon_r = 1$).

Cavities are used as resonators for microwave applications. Therefore, they are comparable to low-frequency resonant circuits consisting of an inductance *L* and a capacitance *C*. In the low-frequency range, lumped elements (inductors and capacitors) are used, which are small in comparison with the wavelength. In contrast, cavities are distributed elements with dimensions comparable to the wavelength. This results in comparatively small losses. Since cavities are distributed elements, it is in general no longer possible to determine *L* and *C* directly. Instead of *L* and *C*, the resonant frequency $f_0 = \omega_0 / 2\pi$ is the most important property of a cavity.

Neither lumped elements nor cavities are completely lossless. One must take into account the finite conductivities of the materials, resulting in a resistance *R* when analyzing resonant circuits. For cavities, however, *R* cannot be determined directly due to the same reasons that hold for *L* and *C*. Therefore, a different parameter, the q-factor *Q* plays a similar role for cavities. *Q* is proportional to the stored electric and magnetic energy *W*, divided by the power loss *P*:

$$Q = \frac{\omega_0 W}{P} \tag{19.15}$$

Although cavities are distributed elements, one is able to show that their behavior near resonance can be described by a simple parallel resonant circuit consisting of *R, L,* and *C* if the reference plane is chosen appropriately. Therefore, the basic properties of such a parallel resonant circuit are analyzed in the following.

Assume that the losses are small ($Q \gg 1$), which is desirable in practice. Therefore, the resistance *R* of the parallel resonant circuit is comparatively large. In this case, the resonant frequency does not depend on *R* in a first-order approximation:

$$\omega_0 \approx 1/\sqrt{LC} \tag{19.16}$$

If Equation 19.15 is applied to the analyzed parallel resonant circuit, one obtains:

$$Q \approx \frac{R}{\omega_0 L} \approx R\sqrt{\frac{C}{L}} \tag{19.17}$$

One can characterize the width of a resonance curve by those angular frequencies $\omega_1 = 2\pi f_1$ and $\omega_2 = 2\pi f_2$ where the power has decreased to one half of its maximum value (–3 dB). The impedance has then decreased to $1/\sqrt{2} \approx 70.7\%$ of its maximum value. This enables calculation of the angular frequencies ω_1 and w_2:

$$\omega_1 \approx \omega_0 - \frac{1}{2RC}, \quad \omega_2 \approx \omega_0 + \frac{1}{2RC} \tag{19.18}$$

Using these relations, one can easily derive the following equation, which is equivalent to Equation 19.17.

$$Q \approx \frac{\omega_0}{\omega_2 - \omega_1} \approx \frac{f_0}{f_2 - f_1} \tag{19.19}$$

This expression shows that *Q* is a symbol for the sharpness of resonance. Furthermore, it leads to the first principle as to how the q-factor can be measured. This principle, which is often referred to as the bandpass method, is based on the measurement of a resonance curve. For example, one can measure the reflection coefficient S_{11} with a network analyzer. From this curve, the 3 dB-bandwidth $\Delta f = f_2 - f_1$ and the resonant frequency $f_0 = (f_1 + f_2)/2$ can be easily determined. The application of Equation 19.19 yields the desired *Q*.

A second principle used to measure the q-factor is based on the transient behavior of the cavity after excitation with a pulse. In this case, the energy decays exponentially, and the time constant of the decay is proportional to Q^{-1}. This can again be shown by analyzing the equivalent parallel resonant circuit. Up until now, all signals were time-harmonic, which enabled a solution by complex quantities. This time, the corresponding differential equation must be solved. One can easily show that the amplitude of the voltage is proportional to $e^{-\omega_0 t/2Q}$, which means a $e^{-\omega_0 t/2Q}$ dependency of the energy exists. Measuring the decay time constant, therefore, enables one to determine the q-factor.

The Q defined here is the unloaded Q of the cavity; that is, no further resistance is connected to the cavity. Sometimes it is desirable to determine the loaded Q (Q_L), which takes into account such resistances. Detailed information about the loaded Q can be found in [21–23]. Although the q-factor is not influenced by the coupling structure if it is lossless, the coupling structure is of great importance. Further information about coupling parameters is presented in [21–23]. Detailed descriptions of measurement methods based on the above mentioned principles can also be found in [21, 22].

Up to now, all analyses were based on the equivalent resonant circuit. There are many other effects that can be explained by this analogy. For example, the energy in both the cavity and in its equivalent circuit oscillates between the magnetic and electric fields. Some properties of cavities, however, can only be seen by examining the electric and magnetic fields themselves. These are governed by Maxwell's equations.

A solution of Maxwell's equations (which can be very complicated for a given cavity) shows that all cavities have an infinite number of resonant frequencies. This could not be seen by analyzing the equivalent parallel resonant circuit. A description of the cavity by a discrete parallel resonant circuit is only valid in the vicinity of *one* of these resonant frequencies.

Furthermore, different modes can exist that have the same resonant frequency. This phenomenon is called *degeneration*. If the resonator will operate at such a frequency, where degenerate modes exist, one has to take care that the companion mode is suppressed. This can be accomplished by an appropriate choice of the positions of the coupling elements.

Even if the desired mode does not have any companion mode, one should take care that no other mode exists in the operating range of the cavity (this can be accomplished with a mode chart [22, 23]); otherwise, these modes must be damped sufficiently in order to be sure that an observed resonance corresponds to the desired mode.

19.5 Scattering Parameter Measurements

Scattering parameters describe multiple port structures in terms of wave variables. The introduction of scattering parameters (*S*-parameters) arises naturally in microwave circuits and systems, due to the lack of a unique definition for currents and voltages at these frequencies. Most circuits and systems at high frequencies are efficiently described in terms of *S*-parameters.

This section describes the fundamentals and properties of *S*-parameters, together with network analysis based on *S*-parameter calculations and measurements. Measurement procedures are outlined and the most frequently used systems for *S*-parameter measurement are described. Finally, information on hardware required for the experimental determination of *S*-parameters is provided, together with the corresponding suppliers.

Introduction and Fundamentals

At high frequencies, the wave variables are a natural extension of the voltages and currents at port terminals. In electric systems where the voltages and currents cannot be uniquely defined, the power flow in a waveguide can be described via wave variables. Whenever a TEM mode of wave propagation cannot be assumed, the currents and voltages are dependent on the integration path. This situation is encountered in all rectangular, circular, and passive waveguide structures, even in the case of lossless wave propagation. It is also true for all guiding structures if losses are to be considered along the path of wave propagation [24–27]. For the case of wave propagation along a transmission line, the wave variables a and b are defined as follows:

$$
\begin{aligned}
a(z) &= \frac{1}{2}\left(\frac{U(z)}{\sqrt{Z_0}} + I(z)\sqrt{Z_0}\right) \\
&= \frac{U_+}{\sqrt{Z_0}} = I_+\sqrt{Z_0} \\
b(z) &= \frac{1}{2}\left(\frac{U(z)}{\sqrt{Z_0}} - I(z)\sqrt{Z_0}\right) \\
&= \frac{U_-}{\sqrt{Z_0}} = I_-\sqrt{Z_0}
\end{aligned}
\tag{19.20}
$$

The propagation is along the z-direction. The characteristic impedance of the transmission line is Z_0, and $U(z)$ and $I(z)$ are the voltage and current, respectively, at location z along the line. The variables $a(z)$ and $b(z)$ are the complex amplitudes of the modes on the line. The voltage U_+ and U_- and the currents I_+ and I_- denote the voltage and current amplitudes, respectively, in forward and reverse direction. The wave variables are related to the power in the following form:

$$
\begin{aligned}
P_+ &= \frac{1}{2}\frac{|U_+|^2}{Z_0} = \frac{1}{2}|I_+|^2 Z_0 = \frac{1}{2}|a(z)|^2 \\
P_- &= \frac{1}{2}\frac{|U_-|^2}{Z_0} = \frac{1}{2}|I_-|^2 Z_0 = \frac{1}{2}|b(z)|^2
\end{aligned}
\tag{19.21}
$$

In Equation 19.21, it is assumed that the system is excited by a pure sinusoid and that the characteristic impedance is purely real. The wave variables have the dimensions of $\sqrt{\text{W}}$.

Strictly speaking, wave variables and S-parameters can only be applied to linear networks. This is important because many publications are devoted to so-called large-signal S-parameter measurements. The interpretation of such results is not simple and great care must be employed in the correct determination of the characteristic impedance of the system [26]. In the case of analysis of large-signal or nonlinear circuits, two methods exist to introduce the wave variables:

- Volterra series representation [28]
- Harmonic-balance method [26]

Both methods transform the nonlinear circuit into a number of linear circuits at different frequencies, and then change the terminal voltages and currents into wave variables. This situation is sketched in Figure 19.9. Particular attention must be paid to the definition of the characteristic impedance, which can vary between different frequencies. An in-depth treatment of wave variables can be found in [26].

A further utilization of wave variables can be found in the noise analysis of microwave circuits. According to Figure 19.10, a noisy multiport can be analyzed by an associated noiseless two-port with the according noise sources c_i at the corresponding ports of the circuit.

Calculations and Analysis with *S*-Parameters

The characterization of multiports with S-parameters requires embedding of the multiport into a system consisting of a signal source with a characteristic impedance and appropriate terminations of all ports. This situation is shown in Figure 19.11. The outgoing wave parameters b are reflections at the corresponding ports. The wave variables are related to the scattering parameters of a two-port in the following manner:

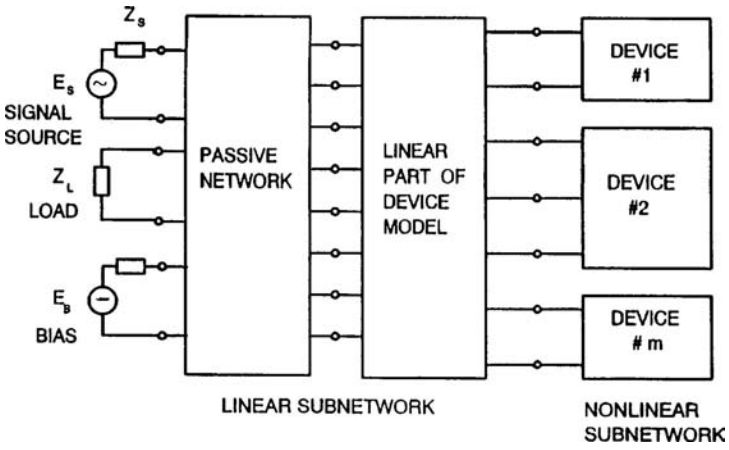

FIGURE 19.9 Schematic illustration of application of wave variables to nonlinear circuits.

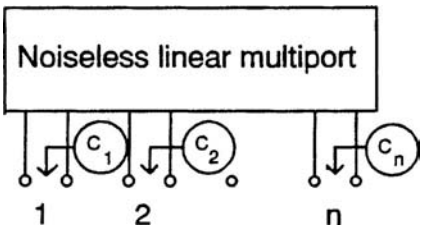

FIGURE 19.10 Schematic illustration of application of wave variables to noisy circuits.

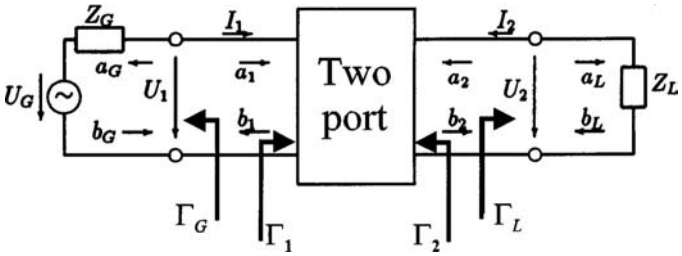

FIGURE 19.11 Two-port network indicating the wave variables and the scattering parameters. The subscripts *G* and *L* indicate the generator and the load, respectively.

$$\begin{pmatrix} b_1 \\ b_2 \end{pmatrix} = (S)\begin{pmatrix} a_1 \\ a_2 \end{pmatrix} = \begin{pmatrix} S_{11} & S_{12} \\ S_{21} & S_{22} \end{pmatrix}\begin{pmatrix} a_1 \\ a_2 \end{pmatrix} \tag{19.22}$$

For the determination of the individual scattering matrix elements, all ports of the network must be terminated in their characteristic impedance. The impedances at the corresponding ports need not be equal for all ports. The *S*-parameters are, in general, complex and are defined with respect to reference planes. These reference planes can be the network terminals, but could also be shifted to other locations in the circuit if this is desirable. The scattering matrix can be transformed into all circuit representations. Table 19.4 indicates the conversion formulae between the *S*-parameters and *Z Y h* parameters for arbitrary characteristic impedances. Additional conversions to *ABCD* and *T* parameters can be found in [29].

TABLE 19.4 Equations for the Conversion Between Different Two-Port Parameters

$$S_{11}=\frac{\left(X_{11}-Z_{01}^{*}\right)\left(X_{22}+Z_{02}\right)-X_{12}X_{21}}{\left(X_{11}-Z_{01}\right)\left(X_{22}+Z_{02}\right)-X_{12}X_{21}} \qquad X_{11}=\frac{\left(Z_{01}^{*}+S_{11}Z_{01}\right)\left(1-S_{22}\right)+S_{12}S_{21}Z_{01}}{\left(1-S_{11}\right)\left(1-S_{22}\right)-S_{12}S_{21}}$$

$$S_{12}=\frac{2X_{12}\sqrt{R_{01}R_{02}}}{\left(X_{11}+Z_{01}\right)\left(X_{22}+Z_{02}\right)-X_{12}X_{21}} \qquad X_{12}=\frac{2S_{12}\sqrt{R_{01}R_{02}}}{\left(1-S_{11}\right)\left(1-S_{22}\right)-S_{12}S_{21}}$$

$$S_{21}=\frac{2X_{21}\sqrt{R_{01}R_{02}}}{\left(X_{11}+Z_{01}\right)\left(X_{22}+Z_{02}\right)-X_{12}X_{21}} \qquad X_{21}=\frac{2S_{21}\sqrt{R_{01}R_{02}}}{\left(1-S_{11}\right)\left(1-S_{22}\right)-S_{12}S_{21}}$$

$$S_{22}=\frac{\left(X_{11}+Z_{01}\right)\left(X_{22}-Z_{02}^{*}\right)-X_{12}X_{21}}{\left(X_{11}+Z_{01}\right)\left(X_{22}+Z_{02}\right)-X_{12}X_{21}} \qquad X_{22}=\frac{\left(1-S_{11}\right)\left(Z_{02}^{*}+S_{22}Z_{02}\right)-S_{12}S_{21}Z_{02}}{\left(1-S_{11}\right)\left(1-S_{22}\right)-S_{12}S_{21}}$$

$$S_{11}=\frac{\left(1-Y_{11}Z_{01}^{*}\right)\left(1+Y_{22}Z_{02}\right)+Y_{12}Y_{21}Z_{01}^{*}Z_{02}}{\left(1+Y_{11}Z_{01}\right)\left(1+Y_{22}Z_{02}\right)-Y_{12}Y_{21}Z_{01}Z_{02}} \qquad Y_{11}=\frac{\left(1-S_{11}\right)\left(Z_{02}^{*}+S_{22}Z_{02}\right)+S_{12}S_{21}Z_{02}}{\left(Z_{01}^{*}+S_{11}Z_{01}\right)\left(Z_{02}^{*}+S_{22}Z_{02}\right)-S_{12}S_{21}Z_{01}Z_{02}}$$

$$S_{12}=\frac{-2Y_{12}\sqrt{R_{01}R_{02}}}{\left(1+Y_{11}Z_{01}\right)\left(1+Y_{22}Z_{02}\right)-Y_{12}Y_{21}Z_{01}Z_{02}} \qquad Y_{12}=\frac{-2S_{12}\sqrt{R_{01}R_{02}}}{\left(Z_{01}^{*}+S_{11}Z_{01}\right)\left(Z_{02}^{*}+S_{22}Z_{02}\right)-S_{12}S_{21}Z_{01}Z_{02}}$$

$$S_{21}=\frac{-2Y_{21}\sqrt{R_{01}R_{02}}}{\left(1+Y_{11}Z_{01}\right)\left(1+Y_{22}Z_{02}\right)-Y_{12}Y_{21}Z_{01}Z_{02}} \qquad Y_{21}=\frac{-2S_{21}\sqrt{R_{01}R_{02}}}{\left(Z_{01}^{*}+S_{11}Z_{01}\right)\left(Z_{02}^{*}+S_{22}Z_{02}\right)-S_{12}S_{21}Z_{01}Z_{02}}$$

$$S_{22}=\frac{\left(1+Y_{11}Y_{11}\right)\left(1-Y_{22}Z_{02}^{*}\right)+Y_{12}Y_{21}Z_{01}Z_{02}^{*}}{\left(1+Y_{11}Z_{01}\right)\left(1+Y_{22}Z_{02}\right)-Y_{12}Y_{21}Z_{01}Z_{02}} \qquad Y_{22}=\frac{\left(Z_{01}^{*}+S_{11}Z_{01}\right)\left(1-S_{22}\right)-S_{12}S_{21}Z_{01}}{\left(Z_{01}^{*}+S_{11}Z_{01}\right)\left(Z_{02}^{*}+S_{22}Z_{02}\right)-S_{12}S_{21}Z_{01}Z_{02}}$$

$$S_{11}=\frac{\left(h_{11}-Z_{01}^{*}\right)\left(1+h_{22}Z_{02}\right)-h_{12}h_{21}Z_{02}}{\left(h_{11}+Z_{01}\right)\left(1+h_{22}Z_{02}\right)-h_{12}h_{21}Z_{02}} \qquad h_{11}=\frac{\left(Z_{01}^{*}+S_{11}Z_{01}\right)\left(Z_{02}^{*}+S_{22}Z_{02}\right)+S_{12}S_{21}Z_{01}Z_{02}}{\left(1-S_{11}\right)\left(Z_{02}^{*}+S_{22}Z_{02}\right)-S_{12}S_{21}Z_{02}}$$

$$S_{12}=\frac{2h_{12}\sqrt{R_{01}R_{02}}}{\left(h_{11}+Z_{01}\right)\left(1+h_{22}Z_{02}\right)-h_{12}h_{21}Z_{02}} \qquad h_{12}=\frac{2S_{12}\sqrt{R_{01}R_{02}}}{\left(1-S_{11}\right)\left(Z_{02}^{*}+S_{22}Z_{02}\right)-S_{12}S_{21}Z_{02}}$$

$$S_{12}=\frac{2h_{21}\sqrt{R_{01}R_{02}}}{\left(h_{11}+Z_{01}\right)\left(1+h_{22}Z_{02}\right)-h_{12}h_{21}Z_{02}} \qquad h_{21}=\frac{2S_{21}\sqrt{R_{01}R_{02}}}{\left(1-S_{11}\right)\left(Z_{02}^{*}+S_{22}Z_{02}\right)-S_{12}S_{21}Z_{02}}$$

$$S_{22}=\frac{\left(h_{11}+Z_{01}\right)\left(h_{22}-Z_{02}\right)-h_{12}h_{21}Z_{02}^{*}}{\left(h_{11}+Z_{01}\right)\left(h_{22}Z_{02}\right)-h_{12}h_{21}Z_{02}} \qquad h_{22}=\frac{\left(1-S_{11}\right)\left(1-S_{22}\right)-S_{12}S_{21}}{\left(1-S_{11}\right)\left(Z_{02}^{*}\right)-S_{12}S_{21}Z_{02}}$$

The scattering parameters in the case of a noisy two-port as indicated schematically in Figure 19.10 are defined as [26]:

$$\begin{pmatrix} b_1 \\ b_2 \end{pmatrix}=\begin{pmatrix} S_{11} & S_{12} \\ S_{21} & S_{22} \end{pmatrix}\begin{pmatrix} a_1 \\ a_2 \end{pmatrix}+\begin{pmatrix} c_1 \\ c_2 \end{pmatrix} \tag{19.23}$$

The noise wave sources c_1 and c_2 represent the noise generated in the circuit and are therefore complex variables varying with time. They are characterized by a correlation matrix C_s as follows:

$$C_s=\overline{\begin{pmatrix} c_1 \\ c_2 \end{pmatrix}\begin{pmatrix} c_1 \\ c_2 \end{pmatrix}^{H}}=\begin{pmatrix} \overline{|c_1|^2} & \overline{c_1c_2^{*}} \\ \overline{c_2c_1^{*}} & \overline{|c_2|^2} \end{pmatrix} \tag{19.24}$$

where the bar indicates times averaging, $(\cdot)_H$ denotes the Hermitian conjugate, and * stands for the complex conjugate.

For the calculation of the cascade connection of two networks, it is desirable to convert the *S*-parameters to *T* parameters defined in the following way:

$$\begin{pmatrix} b_1 \\ a_1 \end{pmatrix} = \begin{pmatrix} T_{11} & T_{12} \\ T_{21} & T_{22} \end{pmatrix} \cdot \begin{pmatrix} a_2 \\ b_2 \end{pmatrix} \tag{19.25}$$

The conversion between *S*-parameters and *T* parameters is given below.

$$T_{11} = S_{12} - \frac{S_{11}S_{22}}{S_{21}} \tag{19.26}$$

$$T_{12} = \frac{S_{11}}{S_{21}} \tag{19.27}$$

$$T_{21} = -\frac{S_{22}}{S_{21}} \tag{19.28}$$

$$T_{22} = \frac{1}{S_{21}} \tag{19.29}$$

It should be emphasized that different definitions of the *T* parameters exist in the literature [2, 24–27, 30]. Power gain, mismatch, insertion loss, etc. can be efficiently described with the help of scattering parameters [2, 30].

Measurement of *S*-Parameters

Network analyzers are generally used for the measurement of *S*-parameters. A schematic configuration of a network analyzer is indicated in Figure 19.12. The network analyzer consists of two structures to separate the signals and a heterodyne receiver. According to the definitions, the measurement is performed in two steps as indicated in Figure 19.13. Different error models are employed for the calibration of the network analyzer. The most simple is the one-port error model, which consists of contributions due to directivity, source mismatch, and frequency response. A flow diagram is illustrated in Figure 19.14.

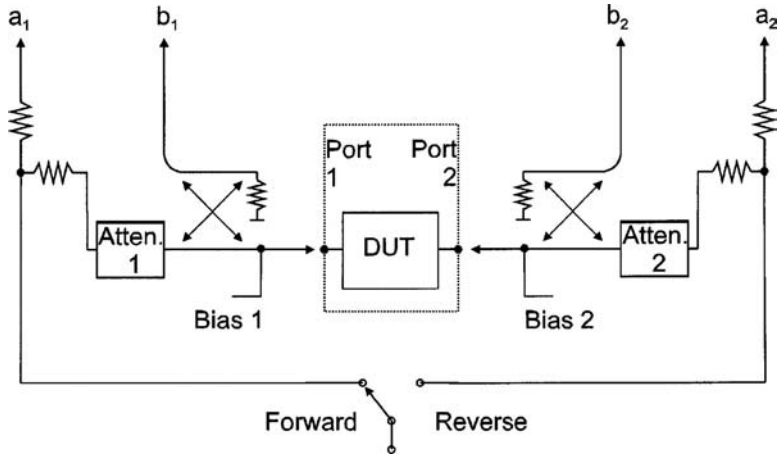

FIGURE 19.12 Schematic illustration of a network analyzer configuration.

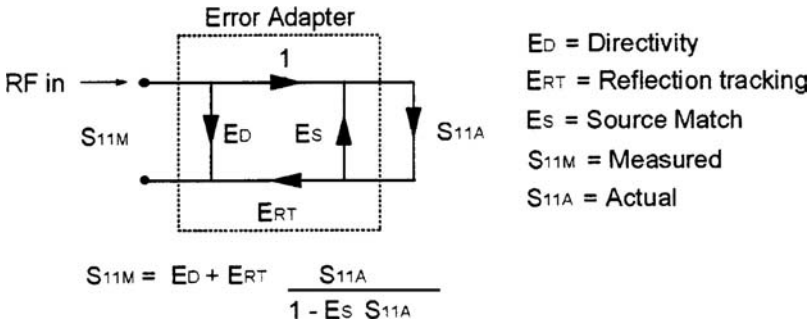

FIGURE 19.13 Flow diagram of the measurement procedure.

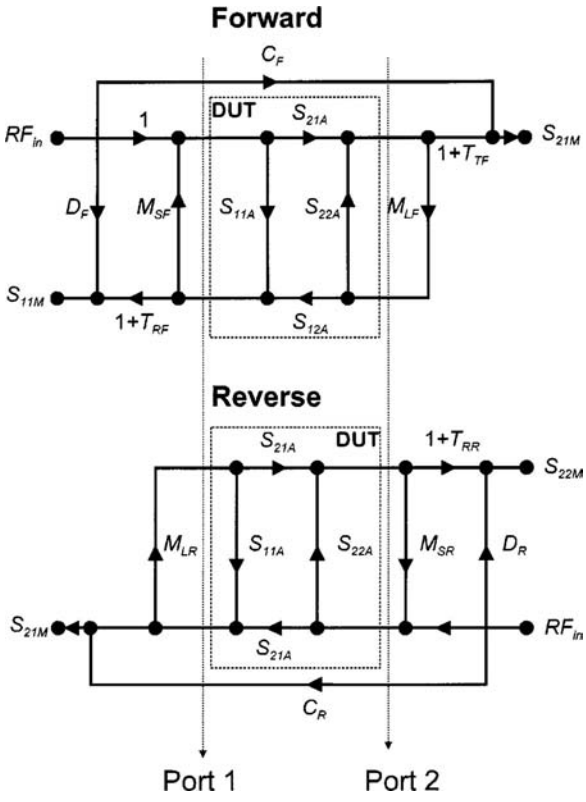

FIGURE 19.14 Flow diagram of the two-port error model.

For the characterization of active and passive two-ports, a more sophisticated error model is required. The signal flow graphs of the full two-port model is drawn in Figure 19.15. To determine the *S*-parameters of the device under test, a de-embedding procedure is required [31–43]. The two-port error model is then divided into two error adapters and the actual device under test (DUT), as depicted in Figure 19.16. The example shown makes reference to the so-called "TRL" calibration procedure. This name abbreviates the three calibration standards utilized in this method: a *through* standard with zero length, a *reflecting* standard, and a *line* standard. This method cannot be applied to on-wafer measurements at low frequencies, due to the excessive line length required for a broadband measurement. Other error correction methods are summarized in Table 19.5 [44]. In addition to the measurements given in the table, a known reference impedance and port 1 to port 2 connection are required. Furthermore, at higher frequencies (above ≈15 GHz), a calibration measurement of the isolation should be performed. For this purpose,

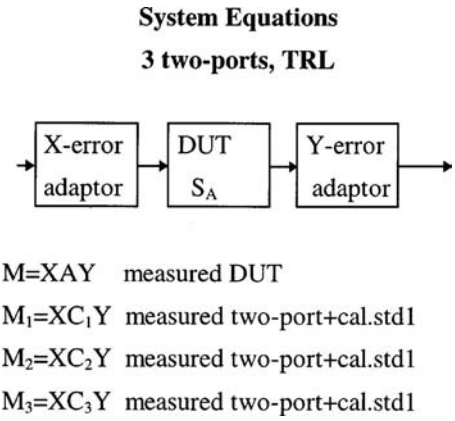

FIGURE 19.15 De-embedding structure for the calibration of a network analyzer.

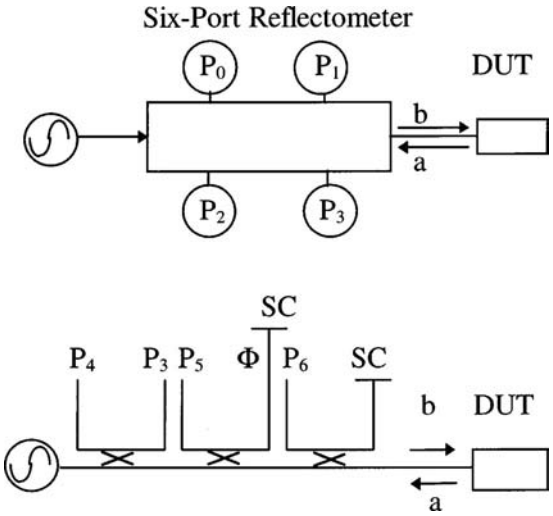

FIGURE 19.16 A network analyzer based on a six-port reflectometer and a possible realization using three couplers and four power detectors, two short-circuits (SC), and one phase shifter (Φ).

TABLE 19.5 Summary of Different Calibration Methods

TOSL	Through standard (T) with known length; Fulfills 4 conditions	3 known reflections (OSL) on port 1; Fulfills 3 conditions	3 known reflections (OSL) on port 2; Fulfills 3 conditions
TRL & LRL	Through or line standard (T) or (L) with known length; Fulfills 4 conditions	Unknown equal reflection standard (R) on port 1 and port 2; Fulfills 1 condition	Line (L) with known S_{11} and S_{22}; Fulfills 2 conditions
TRM & LRM	Through or line standard (T) or (L) with known length; Fulfills 4 conditions	Unknown equal reflection standard (R) on port 1 and port 2; Fulfills 1 condition	Known match (M) on port 1 and port 2; Fulfills 2 conditions
TXYZ & LXYZ	Through or line standard (T) or (L) with known length; Fulfills 4 conditions	3 known reflection standards (XYZ) on port 1 or port 2; Fulfills 3 conditions	
UXYZ	Unknown line standard (U) with $S_{11} = S_{21}$; Fulfills 1 condition	3 known reflection standards (XYZ) on port 1; Fulfills 3 conditions	3 known reflection standards (XYZ) on port 2; Fulfills 3 conditions

TABLE 19.6 Companies Supplying Network Analyzers for *S*-Parameter Measurements

Company	Frequency min	Frequency max	Method	Cal. Methods
Hewlett-Packard HP 8510	45 MHz	110 GHz	Heterodyne	SOLT, TLR, LRL, LRM, TRM
Wiltron	45 MHz	110 GHz	Heterodyne	SOLT, TLR, LRL, LRM, TRM
Rhode & Schwarz	10 Hz	4 GHz	Heterodyne	SOLT, TLR, LTL, LRM, TRM
AB Millimeterique	2 GHz	800 GHz	Heterodyne	TLR, LRL, proprietary

both ports are terminated by their characteristic impedances and a transmission measurement is performed. This measurement determines the values of C_F and C_R in the calibration flow diagram (see Figure 19.14).

Another possibility for performing vector network measurement is based on multiport reflectometers [45]. The advantage of such systems is the reduced complexity of the network analyzer receiver. A possible realization of a reflectometer structure is the so-called *six-port reflectometer*. The reflectometer consists of three couplers and four power sensors. No frequency conversion is required, which simplifies the test equipment.

Commercially Available Network Analyzers

Table 19.6 shows some of the current suppliers for network analysis. The frequency range is 10 Hz up to 800 GHz.

References

1. A. Fantom, *Radio Frequency and Microwave Power Measurements,* London: Peter Peregrinus, 1990.
2. A.L. Lance, *Microwave Measurements* in *Handbook of Microwave Optical Components,* Vol. 1, K. Chang (Ed.), New York: John Wiley & Sons, 1989.
3. J. Minck, Fundamentals of RF and microwave power measurements, Hewlett-Packard Application Note 64-1A, 1997.
4. G.H. Bryant, *Principles of Microwave Measurements,* London: Peter Peregrinus, 1988.
5. *Microwave Powermate,* Marconi Instruments Ltd., 1989.
6. D. Janik, H. Wolf, and R. Schneider, High-Tc edge bolometer for detecting guided millimeter waves, *IEEE Trans. Appl. Superconduct.,* 3, 2148–2151, 1993.
7. P.L. Richards, Bolometers for infrared and millimeter waves, *J. Appl. Phys.,* 76(1), 1–24, 1994.
8. D.M. Rowe, *Handbook of Thermoelectrics,* Boca Raton, FL: CRC Press, 1995.
9. P. Kopystynski, E. Obermayer, H. Delfs, W. Hohenester, and A. Löser, Silicon power sensor from dc to microwave, in *Micro Systems Technologies 90,* Berlin: Springer, 1990, 605–610.
10. G.C.M. Meijer and A.W. Herwaarden, *Thermal Sources,* Bristol: IOP Ltd., 1994.
11. T. Närhi, Nonlinearity characterisation of microwave detectors for radiometer applications, *Electron. Lett.,* 32, 224–225, 1996.
12. F. Wiedmann, B. Huyart, E. Bergeault, and L. Jallet, New structure for a six-port reflectometer in monolithic microwave integrated-circuit technology, *IEEE Trans. Instrument. Measure.,* 46(2), 527–530, 1997.
13. A. Dehé, V. Krozer, B. Chen, and H. L. Hartnagel, High-sensitivity microwave power sensor for GaAs-MMIC implementation, *Electron. Lett.,* 32(23), 2149–2150, 1996.
14. Circuits Multi Projects, *Information CMP — 42*. Grenoble, France, December 1996.
15. Hints for making better spectrum analyzer measurements, Hewlett-Packard Application Note, No. 1286-1, 1997.
16. C. Brown, Spectrum Analysis Basics, *Hewlett-Packard 1997 Back to Basics Seminar,* 1997.

17. A. Kiiss, Microwave instrumentation and measurements, in *Handbook of Microwave Technology,* T.K. Ishii (Ed.), San Diego: Academic Press, 1995, Vol. 2, 562.
18. H. Brand, Spectrum analyzers: precision test instruments, *Microwave J.,* 37(3), 98, 1994.
19. Spectrum analysis: Spectrum analysis basics, Hewlett-Packard Application Note 150, November 1989.
20. T.K. Ishii, Spectrum Analysis: Amplitude and Frequency Modulation, Application Note 150-1, January 1989.
21. M. Sucher and J. Fox, *Handbook of Microwave Measurements,* Vol. II, Polytechnic Press of the Polytechnic Institute of Brooklyn, 1963, chap. VIII.
22. E.L. Ginzton, *Microwave Measurements,* New York: McGraw-Hill, 1957, chap. 7 and 8.
23. F.E. Terman and J.M. Pettit, *Electronic Measurements,* New York: McGraw-Hill, 1952, chapter 4–15.
24. C.A. Lee and G.C. Dalman, *Microwave Devices, Circuits and Their Interaction,* New York: John Wiley & Sons, 1994.
25. G.D. Vendelin, A.M. Pavio, and U.L. Rohde, *Microwave Circuit Design Using Linear and Nonlinear Techniques,* New York: John Wiley & Sons, 1990.
26. J. Dobrowolski, *Microwave Circuit Analysis with Wave Variables,* Norwood, MA: Artech House, 1991.
27. G. Gonzalez, *Microwave Transistor Amplifiers,* Englewood Cliffs, NJ: Prentice-Hall, 1984.
28. D. Weiner and G. Naditch, A scattering variable approach to the Volterro analysis of nonlinear systems, *IEEE Trans. Microwave Theory & Technique,* MTT-24(7), 422–433, 1976.
29. D.A. Frickey, Conversion between S, Z, Y, H, ABSD, and T parameters which are valid for complex source and load impedances, *IEEE Trans. Microwave Theory & Technique,* MTT-42, 205-211, 1994.
30. T.K. Ishii, *Handbook of Microwave Technology,* San Diego, CA: Academic Press, 1995.
31. R.A. Hackborn, An automatic network analyzer system, *Microwave J.,* 45–52, 1968.
32. S. Rehnmark, On the calibration process of automatic network analyzer systems, *IEEE Trans. Microwave Theory & Technique,* MTT-22(4), 457–458, 1974.
33. J. Fitzpatrick, Error models of vector systems measurements, *Microwave J.,* 21(5), 63–66, 1978.
34. D. Rytting, An analysis of vector measurement accuracy enhancement techniques, *RF & Microwave Measurement Symp. and Exhibition,* Hewlett Packard, 1982.
35. N.R. Franzen and R.A. Speciale, A new procedure for system calibration and error removal in automated S-parameter measurements, *5th European Microwave Conf.,* 1975, 69–73.
36. R.A. Soares and C.A. Hoer, A unified mathematical approach to two-port calibration techniques and some applications, *IEEE Trans. Microwave Theory & Techniques,* MTT-37(11), 1669–1674, 1989.
37. R.A. Soares, *GaAs MESFET Circuit Design,* Norwood, MA: Artech House, 1988.
38. Cascade Microtech, *Microwave Wafer Probe Calibration Standards: HP8510 Network Analyzer Input,* Cascade Microtech Instruction Manual, 1990.
39. Understanding the fundamental principles of vector network analysis, Hewlett-Packard Application Note 1287-1, 1997.
40. B. Donecker, Determining the measurement accuracy of the HP8510 microwave network analyzer, *RF & Microwave Measurement Symp. and Exhibition,* Hewlett-Packard, March 1985.
41. Exploring the architectures of network analyzers, Hewlett-Packard Application Note 1287-2, 1997.
42. Applying error correction to network analyzer measurements, Hewlett-Packard Application Note 1287-3, 1997.
43. D. Ballo, Network analyzer basics, *Hewlett-Packard 1997 Back to Basics Seminar,* 1997.
44. H.J. Eul and B. Schiek, Thru-Match-Reflect: one result of a rigorous theory for de-embedding and network analyzer calibration, *18th European Microwave Conf.,* 1988, 909–914.
45. G.F. Engen and C.A. Hoer, Thru-Reflect-Line: an improved technique for calibrating the dual 6-port automatic network analyzer, *IEEE Trans. Microwave Theory & Technique,* MTT-27(12), 993–998, 1979.